Ultrasonics - Sonochemistry 60 (2020) 104798

Contents lists available at ScienceDirect

Ultrasonics - Sonochemistry

journal homepage: www.elsevier.com/locate/ultson

Ultrasound-assisted synthesis of 3D flower-like zinc oxide decorated fMWCNTs for sensitive detection of toxic environmental pollutant 4-nitrophenol

Deepak Balram[a], Kuang-Yow Lian[a,*], Neethu Sebastian[b]

[a] Department of Electrical Engineering, National Taipei University of Technology, No. 1, Section 3, Zhongxiao East Road, Taipei 106, Taiwan
[b] Department of Organic and Polymeric Materials, National Taipei University of Technology, No. 1, Section 3, Zhongxiao East Road, Taipei 106, Taiwan

ARTICLE INFO

Keywords:
Sonochemical
Electrochemical sensor
Zinc oxide
Functionalized multi-walled carbon nanotubes
4-Nitrophenol

ABSTRACT

Sonochemical synthesis of functionalized multi-walled carbon nanotubes (fMWCNTs) embellished 3D flower-like zinc oxide (ZnO) nanocomposite based novel electrochemical sensor for the detection of toxic environmental pollutant 4-nitrophenol (4-NP) is detailed in this paper. We have used laser-assisted synthesis technique in the development of 3D flower-like ZnO nanoparticles (NPs) and ultrasonication method was employed in preparation of ZnO NPs@fMWCNTs nanocomposite using a high-intensity ultrasonic bath DC200H with power of 200 W/cm^2 and 40 KHz frequency. The nanocomposite was meticulously fabricated on screen printed carbon electrode (SPCE) to carry out various electrochemical analysis. Different characterizations such as Raman spectroscopy, Fourier transform infrared (FT-IR) spectroscopy, UV visible spectroscopy (UV–Vis), X-ray diffraction (XRD), scanning electron microscopy (SEM), and high-resolution transmission electron microscopy (HRTEM) of the materials used in this work were taken. Cyclic voltammetry (CV) and differential pulse voltammetry (DPV) techniques are used in electrochemical investigations. We have observed well-defined oxidation and reduction peak currents representing electrochemical mechanism of 4-NP at very low potentials for ZnO NPs@fMWCNTs/SPCE. Furthermore, we were able to achieve efficient electrochemical determination of 4-NP using the developed sensor with a high sensitivity of 11.44 μA μM^{-1} cm^{-2} and very low detection limit (LOD) of 0.013 μM in a broad linear range of 0.06–100 μM. All the significant features of a good sensor including anti-interference, good stability, excellent repeatability, and reproducibility were exhibited by the sensor. Moreover, we have tested practical feasibility of sensor by carrying out real sample analysis on different water samples.

1. Introduction

4-nitrophenol is an aromatic nitro compound used in pesticides production, explosives, drugs, dyes etc. and it appears in nature as a result of wide range of activities. It is considered as a hazardous pollutant and its effective detection is important for environmental safety. The Environmental Protection Agency (EPA), USA lists 4-NP under priority toxic pollutant because of its high toxicity and persistence in nature [1]. 4-NP is mainly present in soil and aquatic environments, commonly in surface water. However, it is difficult to purify water contaminated with organic pollutants with a phenolic structure as they have resistance towards microbial degradation. Moreover, the aerated aqueous solutions of 4-NP can withstand photochemical transformations [2]. Studies shows that 4-NP causes serious health problems including cyanosis, drowsiness, nausea, headache, methemoglobinemia, and eye irritation in human beings [3]. Even at low concentrations, 4-NP causes nasty taste and odor to water. As 4-NP is used in agricultural practices and industries in various forms, its traces are always present in the environment and causes adverse consequences to mankind, animals, and plants [4]. So effective 4-NP detection is crucial and a well-grounded technique to achieve this is a necessity. Various techniques commonly adopted in the detection and separation of 4-NP includes capillary electrophoresis [5], flow-injection [6], gas chromatography [7], and high performance liquid chromatography (HPLC) [8]. But interference with similar compounds, high cost, and complexity are major concerns for these traditional approaches. However, detection based on electrochemical sensors is considered as an efficient method that can overcome all the demerits of aforementioned traditional approaches. The major merits of electrochemical method such as fast response, less complexity, high sensitivity, and miniaturization helps in the selective detection of 4-NP. Hence, in this work we have used electrochemical technique for the effective detection of 4-NP.

* Corresponding author.
E-mail address: kylian@ntut.edu.tw (K.-Y. Lian).

https://doi.org/10.1016/j.ultsonch.2019.104798
Received 10 August 2019; Received in revised form 11 September 2019; Accepted 15 September 2019
Available online 16 September 2019

In electrochemical detection method, the synthesis of right material with excellent electrocatalytic activity for the preparation of modified electrode has prime importance. ZnO is a promising metal oxide and extensive research was carried out in this material for diverse applications. The interest of ZnO in various applications is fueled and fanned by its unique properties including biocompatibility, anti-microbial, photocatalytic, chemical and thermal stability, piezoelectric, optoelectronic etc. [9–12]. The large exciton binding energy (~60 meV) and the broad band gap at room temperature (Eg ~ 3.3 eV) of ZnO are its major advantages over other materials [13]. Moreover, ZnO was effectively utilized in small devices fabrication as it is easy to etch ZnO in every acids and alkalis. Another significant quality of ZnO is that it is environmental friendly. Some of the important diverse application fields of multi-functional ZnO includes biomedical, dye-sensitized solar cells, sensors, transparent electronics, cosmetics, UV-lasers, photodetectors, piezoelectric device, smart windows etc. [14–16 17–19] Morphology of ZnO has significant role in determining its various properties and researches have synthesized different nanostructures of ZnO including nanorods [20], nanoflowers [21], nanospheres [22], nanowires [20], nanotubes [23] etc. Hence it is important to determine new approaches for synthesis of ZnO to attain unique nanostructure with desired properties. Various methodologies are used in the synthesis of ZnO and some of the common methods includes hydrothermal [24], molecular beam epitaxy (MBE) [25], template-based synthesis [26], thermal evaporation [27], melt methods [28] etc. The capability of ZnO to be stable even at higher isoelectric points and the outstanding association of electrons makes ZnO an apt material for electrochemical applications. Nanoparticles have unique physical and chemical properties including catalytic, optical, electrochemical, magnetic etc. Moreover, nanoscale size confers high surface area to nanoparticles. In this context, we have used ZnO nanoaggregates in this work as its large active surface area and good binding characteristic helps in precise molecule determination. Furthermore, as the fabrication of ZnO is comparatively simpler, it is best suited in low cost sensor fabrication. So, ZnO NPs are used in the electrochemical sensor development for 4-NP detection.

Carbon nanotubes (CNTs) are considered as allotropes of carbon with cylindrical structure. It comprises of carbon atoms positioned in a hexagonal grid with ends sealed by hemispherical fullerenes [29]. CNTs are extensively used in various applications because of its excellent electronic, chemical, thermal, dielectric, and mechanical properties [30–33]. The high specific surface area, appropriate pore sizes, and good stability in various conditions makes it best suited to act as a catalyst support. The single-walled and multi-walled carbon nanotubes have attained lot of interest in the field of electrochemistry in recent years and the prime reason behind this interest is its outstanding electrocatalytic property. The tubi-form MWCNTs with excellent chemical stability, higher surface to volume ratio, and good conductivity turns it as a perfect material for electroanalysis [34]. The side wall of MWCNTs allow good support for addition of metal nanoparticles. Studies shows that outstanding catalytic action can be attained using hybrid nanocomposites decorated with CNTs [35,36]. Novel nanocomposites prepared by incorporating metal oxides and CNTs had resulted in high performance with a synergistic effect [37,38]. For instance, CNTs based metal oxide composites exhibited excellent conductivity and microwave attenuation behavior [32,39]. In order to embellish metal nanoparticles uniformly on CNTs surface, we need to pre-functionalize the surface of carbon nanotubes and so we have carried out amine functionalization of MWCNTs in this work. Afterwards, we have combined both ZnO NPs and amine functionalized MWCNTs to prepare a novel nanocomposite for electrochemical application.

New synthetic methods are pivotal in the development of novel advanced nanocomposites with excellent properties. Sonochemical method can be considered as a best method for nanocomposite preparation due to its various advantages. Primarily, sonochemical method is a non-toxic method and hence is a good option in green synthesis approaches. As sonochemical method is comparatively economical and less complex, it is preferred as the fabrication method in recent researches [40,41]. The outstanding physicochemical properties of materials due to the acoustic cavitation effect of sonochemical technique was considered as a major advantage of using this synthetic approach in the preparation of nanocomposites. In sonochemical method, temperature and pressure reaches high values and simultaneous cooling also happens, which helps to drive the physical and chemical reactions [42]. Furthermore, researchers had already reported the porous nature and high specific surface area of nanomaterias prepared by sonochemical approach [43]. It is to be noted that porous nature of nanomaterials aids in the facile diffusion of electrolyte ions and the high specific surface area helps in the enhancement of electrochemical performance of materials [44]. So it's an added advantage when we use sonochemical approach in the preparation of nanocomposites, especially for electrochemical applications.

In this paper, laser-assisted synthesis of novel 3D flower-like ZnO NPs is carried out and is then decorated with fMWCNTs using ultrasonication technique to prepare the nanocomposite for 4-NP determination. The in-depth details of electrochemical determination using ZnO NPs@fMWCNTs/SPCE are explored in this paper in various sections. The laser-assisted flower-like ZnO NPs synthesis, sonochemical synthesis of fMWCNTs and ZnO NPs@fMWCNTs, the characterization results of synthesized materials, and electrochemical experiments conducted as part of the work are described in various sections.

2. Experimental section

2.1. Materials and methods

Monosodium phosphate, 4-NP, MWCNTs, sodium hydroxide, and other chemicals are obtained from Sigma-Aldrich. We have used 0.05 M disodium phosphate and monosodium phosphate solutions in double distilled (DD) water for Phosphate buffer solution (PBS) preparation. We have used AUT 85,177 instrument and a three electrode setup (reference electrode - Ag/AgCl, counter electrode- platinum wire, working electrode – SPCE) for all electrochemical experiments conducted as part of this work. Surface morphology of 3D flower-like ZnO NPs, fMWCNTs, and ZnO NPs@fMWCNTs are evaluated using Hitachi S-4800 field emission scanning electron microscope at 10 KV. Moreover, we have taken HRTEM of ZnO NPs and fMWCNTs using JEM-2100F(HR) field emission electron microscope. Bruker D8 advanced diffractometer was used to analyze the XRD patterns of the synthesized materials used in this study. We have used Dong Woo 500i Raman spectrometer to record the Raman spectrum and PerkinElmer spotlight 200i microspectrometer was used to record the micro-FT-IR spectrum. JASCO V-770 UV–Visible spectrophotometer was used to study the absorbance spectrum as part of the work.

2.2. Laser-assisted synthesis of 3D flower-like ZnO nanoparticles

We have carried out a novel method based on laser light for successful synthesis of novel 3D flower-like ZnO nanoparticles. As first step of this synthesis process, we have mixed 0.05 M $Zn(NO_3)_2 \cdot 6H_2O$ in 100 ml of DD water and 3 M NaOH in 20 ml DD water. Afterwards, solutions are carefully mixed together. After appropriate mixing of the solutions, we have applied laser light to the mixture solution for 90 min. Then, the resultant white product from the process was fetched using centrifugation method. We have washed this fetched white product thoroughly using DD water and ethanol. In the final stage, this washed material is dried in air oven at 70 °C to get 3D flower-like ZnO NPs.

2.3. Sonochemical synthesis of fMWCNTs

In the synthesis of amine functionalized MWCNTs, we have thoroughly mixed 25 mg of MWCNTs with 250 ml of DD water as the initial step. This mixture solution is then sonicated for 80 min at room

temperature. After sonication process, we have carefully added L-cysteine solution to the prepared MWCNT mixture. This new mixture is again sonicated for 45 min. Then, at room temperature, magnetic stirring of the sonicated mixture for 2.5 hrs is carried out. The black color material we got after stirring process was centrifuged and washed thoroughly to remove extra bound cysteine. The final fMWCNTs was obtained by drying the washed product in an air oven.

2.4. Sonochemical synthesis of ZnO NPs@fMWCNTs and its fabrication on SPCE

We have prepared ZnO NPs@fMWCNTs nanocomposite based on sonochemical technique. As the initial step, 30 mg prepared ZnO NPs was mixed in DD water. This solution is then sonicated for 40 min using ultrasonic bath DC200H (200 W/cm^2, 40 KHz). Then, 10 mg sonochemically synthesized fMWCNTs are added to sonicated solution. Magnetic stirring is performed on this mixture. In order to get the final ZnO NPs@fMWCNTs nanocomposite, the solution is then ultra-sonicated for 2.5 hrs.

As the initial step of fabrication, the prepared ZnO NPs@fMWCNTs nanocomposite was dispersed in ethanol (3 mg/mL; ethanol) using ultrasonication technique. This is followed by the careful drop cast of 8 μL dispersed solution on SPCE. Then, ZnO NPs@fMWCNTs modified SPCE was dried in oven at 30 °C. Afterwards, for removal of unattached ZnO NPs@fMWCNTs on the dried SPCE surface, we gently washed using DD water. After the fabrication of ZnO NPs@fMWCNTs on SPCE, we have used it in the electrochemical experiments to determine 4-NP. The schematic portrayal of sonochemical preparation of ZnO NPs@fMWCNTs and fabrication on SPCE is presented in Scheme 1.

3. Results and discussions

3.1. Characterization

We have analyzed XRD of 3D flower-like ZnO NPs in this work. Fig. 1 denotes the XRD patterns of the synthesized 3D flower-like ZnO NPs and JCPDS card (36–1451) of pure ZnO. Characterization of the crystal structure of ZnO NPs shows well-defined diffraction peaks at

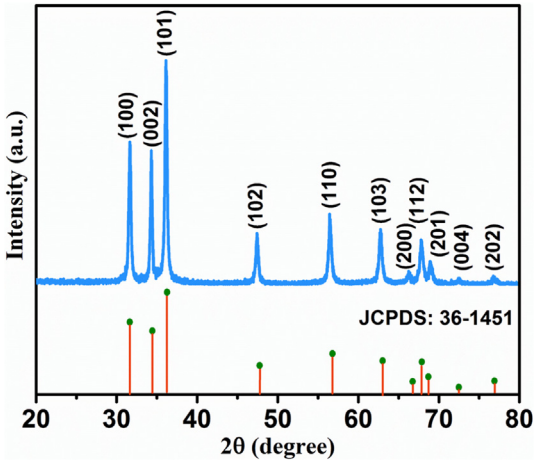

Fig. 1. The XRD pattern of 3D flower-like ZnO NPs.

31.64, 34.31, 36.11, 47.39, 56.42, 62.75, 66.23, 67.78, 68.89, 72.58, and 76.74 representing the various diffraction planes (1 0 0), (0 0 2), (1 0 1), (1 0 2), (1 1 0), (1 0 3), (2 0 0), (1 1 2), (2 0 1), (0 0 4), and (2 0 2) respectively. When we analyze the resultant diffraction peaks, it is evident that it accurately matches to the wurtzite hexagon structure of pure ZnO [45]. This indicates good crystalline characteristic of the synthesized ZnO without impurities. We have used Debye-Scherrer equation mentioned in Eq. (1) to evaluate the grain size of 3D flower-like ZnO NPs:

$$X_G = \frac{k\lambda}{\beta cos\Theta} \tag{1}$$

where $X_G$denotes the grain size, k is the Scherrer's constant, λ represents the incident x-ray wavelength, β is the integral half width, andΘ denotes the Bragg angle. The calculated grain size from the resultant XRD data is 25.84 nm [39].

Surface morphological investigation of 3D flower-like ZnO NPs, fMWCNTs, and ZnO NPs@fMWCNTs was carried out using SEM. SEM images at various magnifications are denoted in Fig. 2. When we

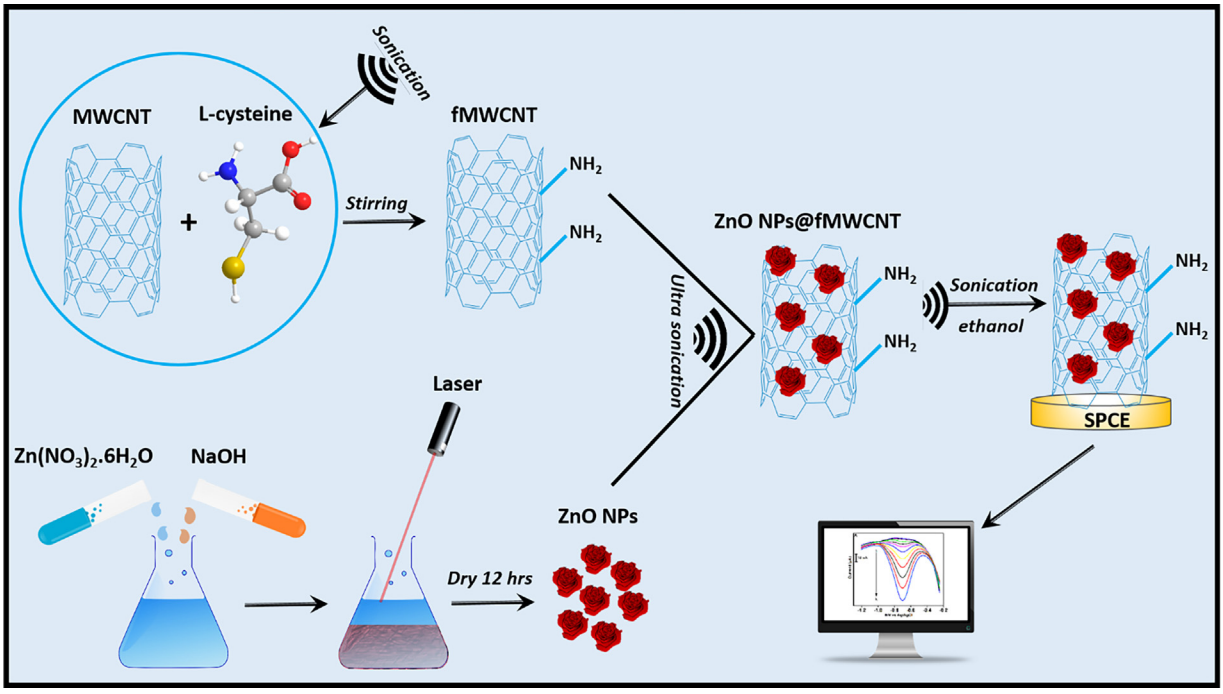

Scheme 1. Schematic portrayal of sonochemical preparation of ZnO NPs@fMWCNTs/SPCE and its application in 4-NP determination.

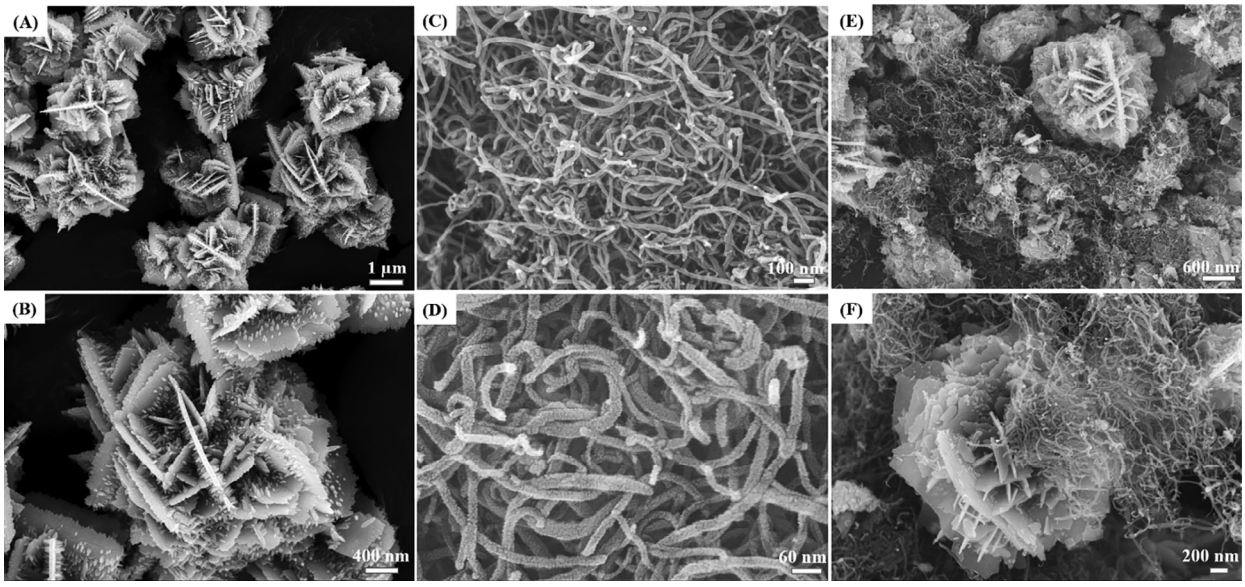

Fig. 2. SEM under different magnification: (A-B) 3D flower-like ZnO NPs; (C-D) fMWCNTs; (E-F) ZnO NPs@fMWCNTs.

analyze the SEM image of ZnO NPs, we can visualize a 3D flower-like structure with many sharp edged petals arranged randomly. We have estimated the diameter of ZnO from resultant SEM and found it to be 2–3 µm. The investigation of surface morphology of fMWCNTs as in Fig. 2C and D shows thin tube-like structure. The mean diameter of each tube ranges between 20 and 30 nm. Furthermore, we have analyzed the SEM images of ZnO NPs@fMWCNTs as given in Fig. 2E and F. Presence of 3D flower-like ZnO and tubi-form fMWCNTs arranged randomly in the SEM image indicating the proper connection between both in the prepared nanocomposite can be visualized.

The disorder and flaws of carbon materials can be effectively investigated using Raman spectroscopy. Hence, Raman spectra investigation of 3D flower-like ZnO NPs, fMWCNTs, and ZnO NPs@fMWCNTs are conducted. The Raman spectrum of 3D flower-like ZnO NPs is shown in Fig. 3A. When we analyze the spectra, we can see a strong and well-defined peak at 422 cm^{-1} because of the oxygen ion vibrations in ZnO and it represents the E_2 high mode. This particular mode is the strongest that represents wurtzite crystal structure of ZnO and hence its well-defined presence in Raman spectra of 3D flower-like ZnO proves its excellent crystallinity. Furthermore, we can find two more peaks in Raman spectra of 3D flower-like ZnO at 558 cm^{-1} and 1139 cm^{-1}. These peaks represent 1st order and 2nd order longitudinal optical modes of ZnO formed due to unoccupied oxygen positions in ZnO. These two optical modes are denoted as E_1 LO and E_2 LO and its presence in Raman spectra of 3D flower-like ZnO further proves its good crystallinity and wurtzite crystal structure [46]. When we analyze the Raman spectra of fMWCNTs shown in Fig. 3B, we can find strong peaks at 1365 cm^{-1}, 1604 cm^{-1}, and 2694 cm^{-1} representing D band, G band, and 2D band respectively. The D band represents the sp^3 disordered carbon band and the G band represents sp^2 graphitic carbon band [47]. All the three peaks of fMWCNTs and the E_2 LO mode of ZnO can be visualized in Raman spectra of ZnO NPs@fMWCNTs shown in Fig. 3B. So the peaks at 1198 cm^{-1}, 1404 cm^{-1}, 1636 cm^{-1}, and 2677 cm^{-1} in ZnO NPs@fMWCNTs Raman spectra represents the E_2 LO mode of ZnO, D band, G band, and 2D band of fMWCNTs respectively and only a slight shift is there in all these peaks indicating good interaction of ZnO and fMWCNTs in the prepared nanocomposite. It is to be noted that the E_2 LO mode of ZnO is suppressed in the case of Raman spectra of ZnO NPs@fMWCNTs nanocomposite due to the interaction with fMWCNTs. Furthermore, the I_D/I_G ratio of fMWCNTs and ZnO NPs@fMWCNTs is calculated to study the disorder degree. The estimated I_D/I_G of fMWCNTs and ZnO NPs@fMWCNTs is 1.01 and 1.04 respectively. The higher I_D/I_G of ZnO NPs@fMWCNTs compared to fMWCNTs indicates its higher disorder degree due to the addition of ZnO [48].

Evaluation of presence of characteristic groups in a material is

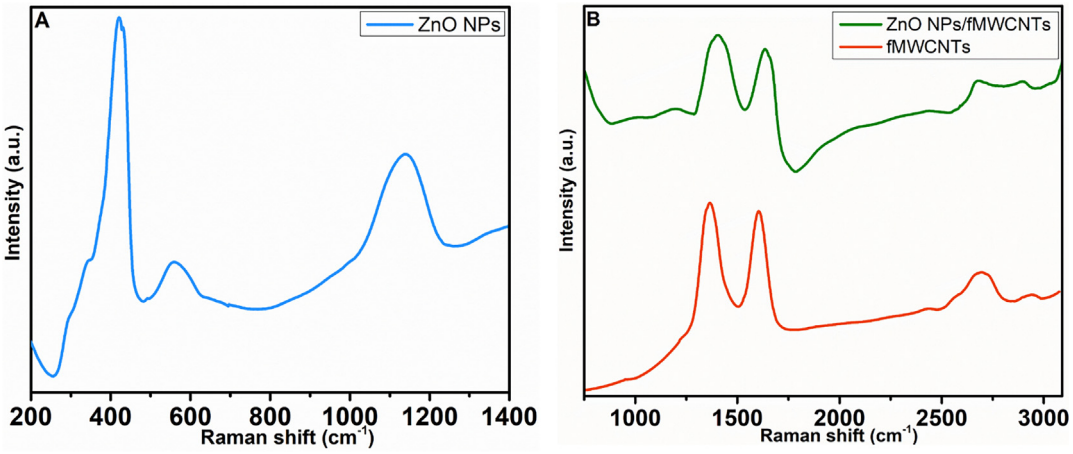

Fig. 3. (A) Raman spectra of ZnO NPs; (B) fMWCNTs and ZnO NPs@fMWCNTS.

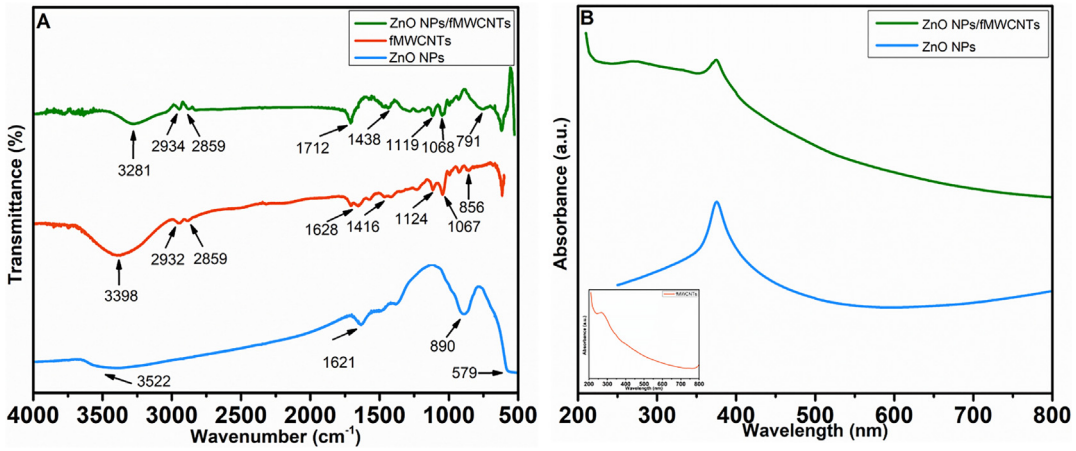

Fig. 4. (A) Micro FT-IR spectra and (B) UV–Vis spectra of ZnO NPs, fMWCNTs, and ZnO NPs@fMWCNTs. Inset UV–Vis spectrum of fMWCNTs.

important and hence we have performed FT-IR spectroscopy studies in 3D flower-like ZnO NPs, fMWCNTs, and ZnO NPs@fMWCNTs. The analysis of FT-IR spectrum of ZnO in Fig. 4A, shows a high intense band at 579 cm^{-1} representing stretching vibrations of oxygen and zinc in ZnO. The peak at 890 cm^{-1} denotes the Zn-OH stretching vibration. The bands at 1621 cm^{-1} and 3522 cm^{-1} corresponds to bending and stretching vibrations of O–H. So, all characteristic bands of ZnO can be clearly seen in FT-IR spectra of 3D flower-like ZnO indicating its correct synthesis [49–51]. We have also evaluated the FT-IR spectra of fMWCNTs as part of this work and is depicted in Fig. 4A. The stretching vibrations due to N–H bond of amine group as a result of fMWCNTs functionalization is represented by the peak at 1628 cm^{-1} and –NH stretching overlapped with O–H vibrations is denoted by the characteristic peak at 3398 cm^{-1}. The peaks at 2932 cm^{-1} and 2859 cm^{-1} represent the C-H stretching vibrations. Furthermore, the peaks at 1416 cm^{-1} and 1124 cm^{-1} represent C-N stretching vibrations and the C = C stretching vibrations corresponds to the peak at 1067 cm^{-1}. Moreover, peak obtained at 856 cm^{-1} denotes the out of plane NH_2 bending mode [52]. When we consider FT-IR spectra of ZnO NPs@fMWCNTs, similar peaks can be visualized as in fMWCNTs at 3281 cm^{-1}, 2934 cm^{-1}, 2859 cm^{-1}, 1712 cm^{-1}, 1438 cm^{-1}, 1119 cm^{-1}, and 1068 cm^{-1}. Also, the peak at 791 cm^{-1} represents the characteristic band of ZnO NPs corresponding to Zn-OH stretching vibrations. There is a slight shift in peak position of all these peaks in FT-IR spectrum of ZnO NPs@fMWCNTs comparing to that of fMWCNTs and ZnO. This shift is because of coincidence of bands due to the interaction of ZnO NPs and fMWCNTS. So it is evident that the characteristic bands of both 3D flower-like ZnO NPs and fMWCNTs are present in FT-IR spectrum of ZnO NPs@fMWCNTs indicating outstanding association and dispersion between ZnO NPs and fMWCNTs in nanocomposite.

We have examined the concentration of absorbing species in UV visible spectra by carrying out UV–Vis spectroscopy of ZnO NPs, fMWCNTs, and ZnO NPs@fMWCNTs. Analysis of UV–Visible spectroscopy of ZnO NPs as in Fig. 4B shows a high intense band at 377 nm. This characteristic peak denotes the band edge absorption of ZnO and is a proof for perfect evolution of ZnO nanoparticles following the synthesis method carried out in this work [53]. We have taken the UV–Vis spectra of fMWCNTs and is shown in Fig. 4B as inset. We can visualize a well-defined peak at 268 nm denoting the characteristic peak of fMWCNTs when we analyze the UV–Vis of fMWCNTs [54]. Moreover, we have analyzed UV–Vis spectrum of ZnO NPs@fMWCNTs also in this work. The resultant UV–Vis spectra show two peaks, at 269 nm and 377 nm, similar to the peaks of fMWCNTs and ZnO NPs respectively. This is an evidence for the existence of fMWCNTs and ZnO in the prepared nanocomposite. Furthermore, when we take into consideration the absorbance rate, we can find that it is higher for ZnO NPs@fMWCNTs than fMWCNTs and ZnO NPs. In other words, decoration of fMWCNTs on ZnO NPs improved its absorbance rate. So this newly synthesized ZnO NPs@fMWCNTs with high absorbance rate can be utilized in various applications.

3.2. Electrochemical performance of ZnO NPs@fMWCNTs nanocomposite

We have compared the cyclic voltammetric behavior of the developed ZnO NPs@fMWCNTs/SPCE with other electrodes towards the detection of 4-NP in the initial stage of electrochemical performance evaluation. Fig. 5A depicts the resultant cyclic voltammograms of the unmodified SPCE (a), ZnO NPs/SPCE (b), fMWCNTs/SPCE (c), and ZnO NPs@fMWCNTs/SPCE (d) in the presence of 200 μM 4-NP in 0.05 M PBS (pH 7.0) at a scan rate of 100 mV/s. The peak current of unmodified SPCE as in Fig. 5A is almost negligible. Even though fMWCNTs/SPCE and ZnO NPs/SPCE showed some electrocatalytic activity towards 4-NP determination, their peak currents are not as high as that of ZnO NPs@fMWCNTs/SPCE. The peak current representing the irreversible reduction of 4-NP to 4-hydroxyaminophenol at ZnO NPs@fMWCNTs/SPCE is almost 5.26 times that of unmodified SPCE which indicates that the electron transfers between ZnO NPs@fMWCNTs/SPCE and electrolyte is faster than other compared electrodes. The large surface area of ZnO NPs@fMWCNTs/SPCE compared to unmodified SPCE is one of the reason for this enhancement in the reduction current. Moreover, lowest peak potentials are also achieved in the case of ZnO NPs@fMWCNTs/SPCE compared to all other electrodes considered in this experiment. This low peak potential is achieved because all the substrate at the ZnO NPs@fMWCNTs electrode surface has been oxidized and reduced faster compared to other modified electrodes because of its high electrocatalytic property. The excellent electrocatalytic performance of ZnO NPs@fMWCNTs/SPCE than all other electrodes we compared in this experiment is evident from its high peak current and low peak potential. This high performance of ZnO NPs@fMWCNTs/SPCE compared to other electrodes is because of the synergistic effect between ZnO NPs and fMWCNTs. The electrochemical mechanism of 4-NP involving its reduction to 4-hydroxyaminophenol and redox process between 4-hydroxyaminophenol and 4-nitrosophenol is shown in scheme 2.

3.2.1. Effect of pH on ZnO NPs@fMWCNTs/SPCE

It is essential to evaluate pH influence in electrochemical process and hence we have performed cyclic voltammetry experiment to determine the influence of various pH values in 4-NP detection based on ZnO NPs@fMWCNTs/SPCE. Fig. 5B depicts different cyclic voltammetry curves recorded at ZnO NPs@fMWCNTs/SPCE towards 4-NP electrochemical reduction under different pH solutions. We have carried out this experiment in presence of 200 μM 4-NP at a fixed scan rate

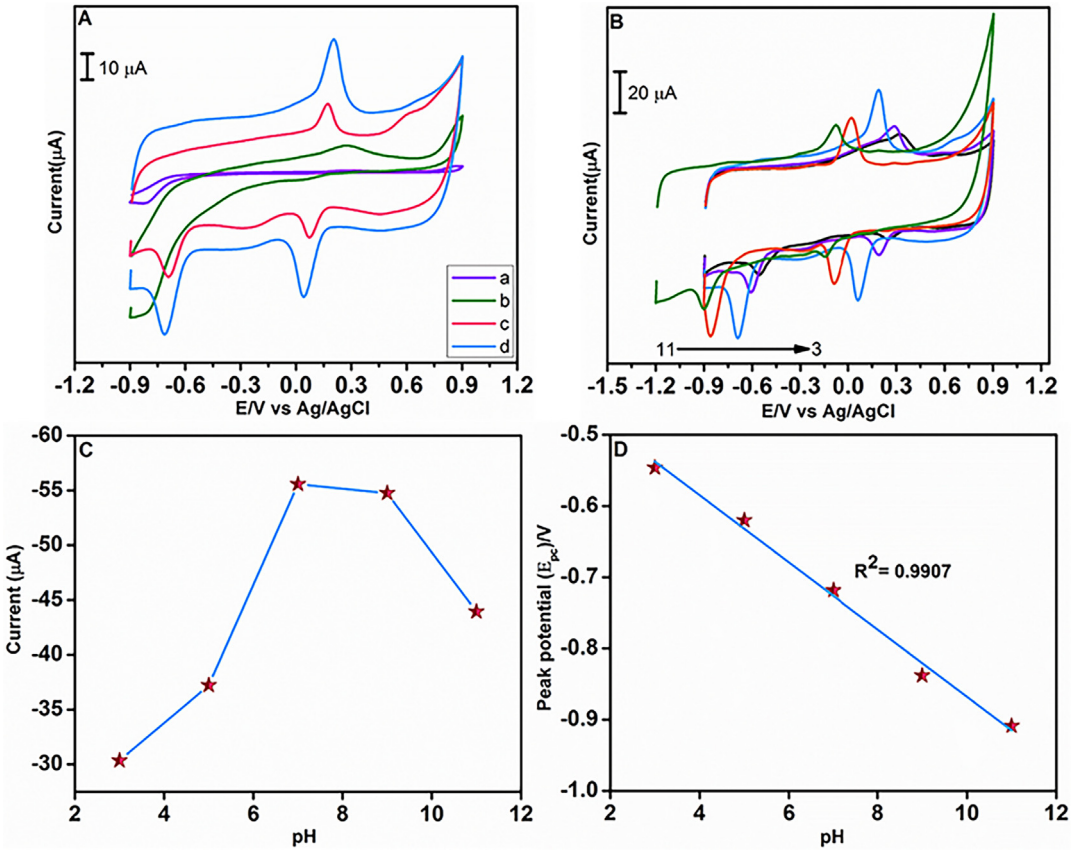

Fig. 5. (A) Cyclic voltammetry responses of unmodified SPCE (a), ZnO NPs/SPCE (b), fMWCNTs/SPCE (c), and ZnO NPs@fMWCNTs/SPCE (d) comprising 200 µM 4-NP in 0.05 M PBS. (B) Cyclic voltammetry responses of ZnO NPs@fMWCNTs/SPCE in various pH solutions having 200 µM 4-NP. (C) Plot of pH against cathodic peak current. (D) Plot of pH against peak potential.

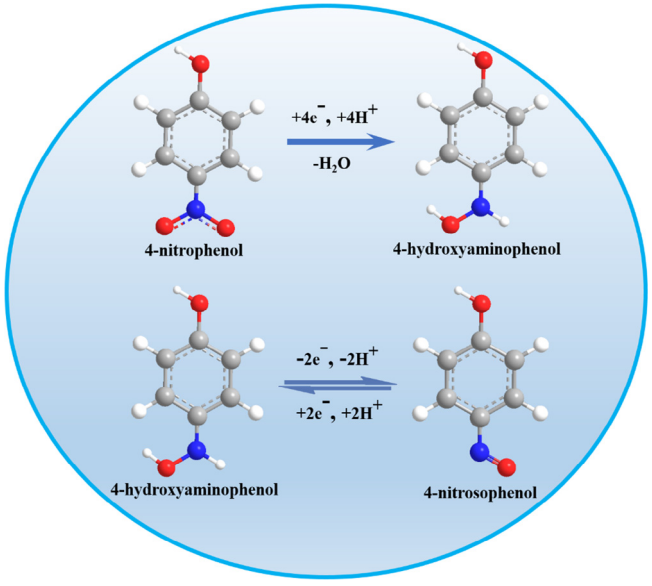

Scheme 2. Electrochemical mechanism of 4-NP at ZnO NPs@fMWCNTs/SPCE.

of 100 mV/s. When cyclic voltammetry curves in Fig. 5B is analyzed, it is noted that peak currents increase from pH 3.0 to pH 7.0 and gradually decreases from pH 7.0 to 11.0. The highest peak currents are obtained for pH 7.0 comparatively. Moreover, when we look into the peak potentials of the resultant cyclic voltammetry curves under different pH solutions, we can find that the peak potentials reduce from pH 3.0 to pH 11.0. This behavior is because of protons involvement in electrocatalytic mechanism of 4-NP. Fig. 5C shows the linear relationship between pH of the detection medium and reduction peak current. We have plotted a linear graph between pH and reduction peak potential and is depicted in Fig. 5D. We have derived linear regression equation from the linear plot depicted in Fig. 5D to estimate the slope value. The resultant linear regression equation is E_{pc} (V) = −0.0471pH − 0.3958 (R^2 = 0.9907) and the estimated slope value is 47.1 mV per pH signifying the participation of same number of electrons and protons in the process according to Nernst equation [55,56]. From this pH evaluation experiment, it is evident that pH 7.0 is the most stable pH with high response to further carry out electrochemical experiments. So we have selected pH 7.0 as the detection medium to perform all the electrochemical experiments in this work.

3.2.2. *Effect of concentration and scan rate on ZnO NPs@fMWCNTs/SPCE*

The cyclic voltammograms of ZnO NPs@fMWCNTs/SPCE in PBS (pH 7.0) at a fixed scan rate of 100 mV/s with different 4-NP additions from 50 to 500 µM is shown in Fig. 6A. Analyzing the figure, we can see a steady linear enhancement in redox peak currents with 4-NP addition to the detection medium. The calibration plot representing this linear relationship between addition of 4-NP and the cathodic peak current is depicted in Fig. 6B. We have determined the cathodic linear regression equation from the respective calibration plot and is found to be y = −0.4614x + 12.734 (R^2 = 0.9904). This experiment to evaluate the effect of concentration resulted in the demonstration of excellent performance of the ZnO NPs@fMWCNTs/SPCE towards 4-NP detection.

In the next stage, we have investigated the effect of scan rate in 4-NP detection based on ZnO NPs@fMWCNTs/SPCE. In order to achieve this, experiment at varied scan rates ranging 20 mV/s to 200 mV/s in 0.05 M PBS containing 200 µM 4-NP was performed. The resultant cyclic voltammetry responses we attained are represented in Fig. 6C. It

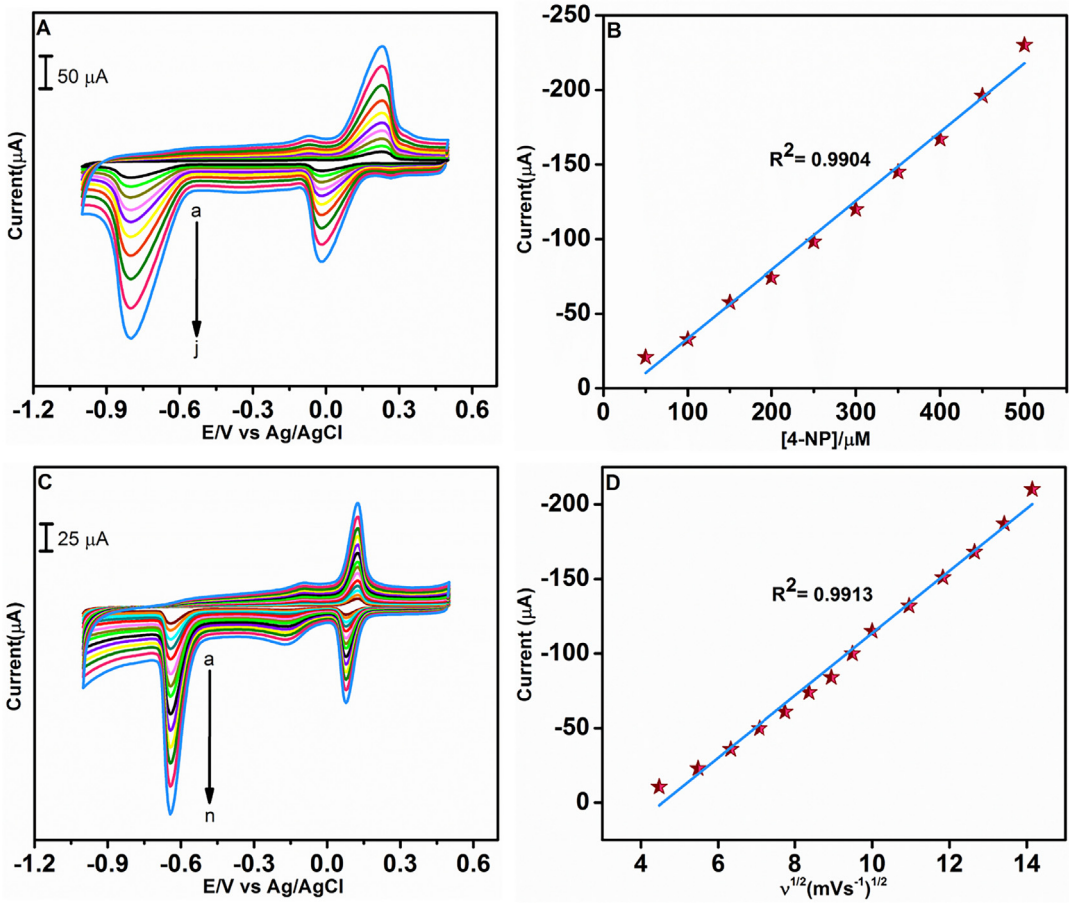

Fig. 6. (A) Cyclic voltammetry response of ZnO NPs@fMWCNTs/SPCE under different concentrations of 4-NP. (B) Plot of cathodic peak current against 4-NP concentration. (C) Cyclic voltammetry response of ZnO NPs@fMWCNTs/SPCE in 200 μM 4-NP under different scan rates. (D) Plot of cathodic peak current against square root of scan rate.

is noted that peak currents linearly increase with scan rate as we evaluated the resultant cyclic voltammetry response. This linear dependency can be further visualized when we evaluate the corresponding calibration plot of reduction peak current against square root of scan rate given in Fig. 6D. We have determined linear regression equation and found to be $I_{pc} = -20.8814x + 95.114$ (μA, mV s^{-1}, $R^2 = 0.9913$). The aforementioned outcome from this experiment indicates that the electrochemical reduction process of 4-NP at ZnO NPs@fMWCNTs/SPCE is a diffusion controlled process [57].

3.2.3. Comparative analysis of electroactive surface area

Electroactive surface area has greater influence in the electrochemical performance and hence it is essential to examine the electroactive surface area of a material to know its suitability in electrochemical applications. So we have conducted studies to evaluate electroactive surface area of ZnO NPs@fMWCNTs/SPCE. As part of the experiment, a comparative analysis of cyclic voltammetry responses of unmodified SPCE and ZnO NPs@fMWCNTs/SPCE is carried out using 0.1 M KCl comprising 5 mM $[Fe(CN)_6]^{-3/-4}$ solution at various scan rates between 20 and 200 mV s^{-1}. Fig. 7A and 7C depicts cyclic voltammetry curves obtained from this experiment for bare SPCE and ZnO NPs@fMWCNTs/SPCE respectively. The corresponding linear plots showing the relationship between square root of scan rate and redox peak currents are given in Fig. 7B and D. The slope value is estimated from the resultant plots and Randles Sevcik equation given below is used to estimate electroactive surface area of electrodes [58]:

$$I_p = (2.69 \times 10^5) A D^{1/2} \nu^{1/2} n^{3/2} C \quad (2)$$

where I_p is the oxidation peak current; the electrons participated in the process is represented by n; A refers to active surface area of the electrode; D denotes diffusion coefficient (mol/cm^3); C represents the concentration; and ν is the scan rate. The active surface area of unmodified SPCE and ZnO NPs@fMWCNTs/SPCE estimated from Randles Sevcik equation are 0.058 and 0.148 respectively. So the electroactive surface area of ZnO NPs@fMWCNTs/SPCE is 2.5 times that of bare SPCE. This shows the superior electrocatalytic activity of ZnO NPs@fMWCNTs/SPCE towards 4-NP detection.

3.2.4. Electrochemical determination of 4-NP by DPV technique

We have performed electrochemical detection of 4-NP based on ZnO NPs@fMWCNTs/SPCE using DPV technique because of its high sensitivity and efficiency. The differential pulse voltammetric responses of ZnO NPs@fMWCNTs/SPCE towards 4-NP detection are recorded. In this experiment, 4-NP determination is carried out at different solution concentrations and the resultant sharp DPV curves are shown in Fig. 8A. The cathodic peak current has increased with each addition of 4-NP showing a linear dependency and the corresponding plot is shown in Fig. 8B. We can see that there is no variation in the peak potential even as the 4-NP concentration increases denoting good efficiency for proposed nanocomposite. The linear regression equation is estimated from the linear plot and is found to be I (μA) = -0.8340x − 23.3779 with a Pearson correlation coefficient of 0.9924 in the linear range of 0.06–100 μM. An ultra-low LOD value of 0.013 μM and a good sensitivity of 11.44 μA μM^{-1} cm^{-2} are resulted according to DPV response indicating excellent performance of the developed ZnO NPs@fMWCNTs/SPCE in the detection of 4-NP. Furthermore, we have made a comparative investigation of performance of ZnO NPs@fMWCNTs/

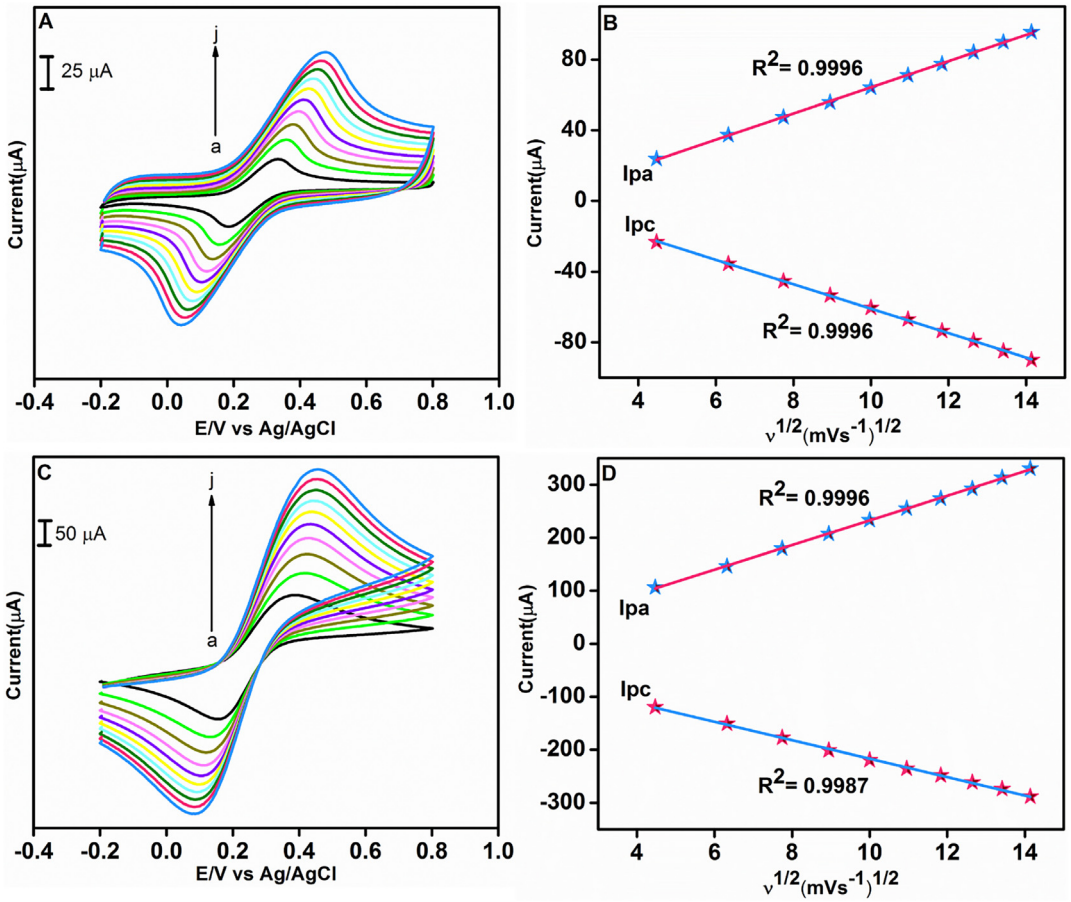

Fig. 7. Cyclic voltammogramms in 0.1 M KCl having 5 mM $[Fe(CN)_6]^{-3/-4}$ under various scan rates at (A) bare SPCE and (C) ZnO NPs@fMWCNTs/SPCE. Calibration plot of redox peak currents vs square root of scan rate at (B) bare SPCE and (D) ZnO NPs@fMWCNTs/SPCE.

SPCE with other modified electrodes based on LOD and linear range and is given in Table 1. When we analyze Table 1, we can clearly recognize that ZnO NPs@fMWCNTs is an apt material for detection of hazardous pollutant 4-NP.

3.2.5. *Selectivity, reproducibility, stability and repeatability*

The existence of concomitant species at any phase of electrochemical detection can inhibit performance of electrochemical sensor due to interference problems. The selectivity of the ZnO NPs@fMWCNTs based sensor was investigated to make sure that no interference issues exists in the electrochemical detection of 4-NP. We have used DPV technique to investigate the anti-interfering property of the proposed sensor and is carried out in PBS containing 10 μM 4-NP. The change in current response of 4-NP is examined in the existence of common interfering compounds including phenol derivatives as part of the work. We have conducted this performance analysis using 10-fold excess concentration of 2-nitrophenol (2-NP), 3-nitrophenol (3-NP), nitrobenzene (NB), hydroquinone (HQ), catechol (CC), resorcinol (RC) and 50-fold excess concentration of copper (Cu^{2+}), nickel (Ni^{2+}), manganese (Mn^{2+}), chlorine (Cl^-), and sulfate (SO_4^{2-}). Fig. 9A shows

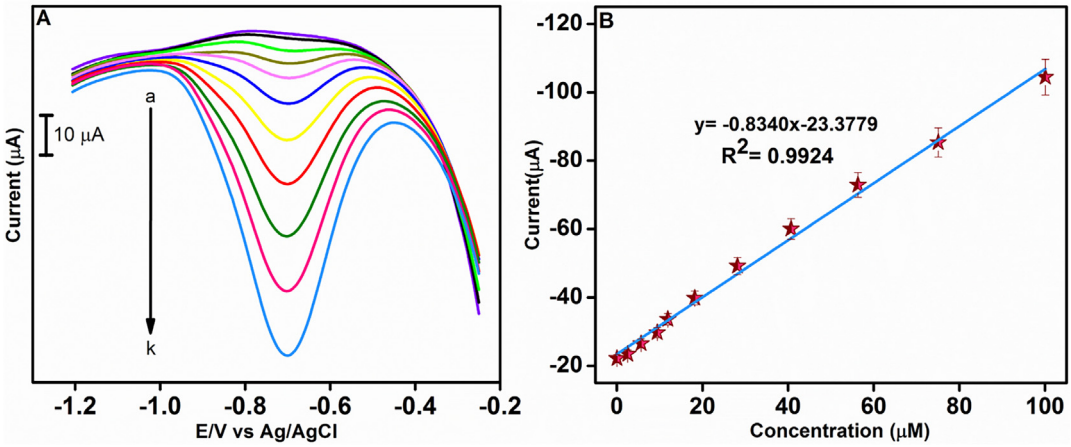

Fig. 8. (A) DPV responses for the addition of 4-NP in 0.05 M PBS (pH 7.0) under various concentrations at ZnO NPs@fMWCNTs/SPCE. (B) Linear plot of peak current response against concentration of 4-NP.

Table 1
Comparative performance evaluation of ZnO NPs@fMWCNTs/SPCE.

Modified electrode	Detection technique	LOD (μM)	Linear range (μM)	pH	References
Nano-Au/GCE	SDV	8.0	10–1000	6	[59]
Co_3O_4/GCE	SWV	0.93	2.0–5.0	7	[60]
HA-NP/GCE	Amperometry	0.6	1.0–300	7	[61]
β-CD/RGO/GCE	DPV	0.36	7.19–71.89	4	[62]
GC-UNFE	CV	0.23	0.5–3000	7	[63]
FeO_x/TiO_2@mC	Amperometry	0.183	5–310	7	[64]
Cu_2O-Pt RRDE	DPV	0.1	10–100	5.8	[65]
Au-Cu NPs/GCE	DPV	0.08	0.1–15	5	[66]
nAg-chitosan/GCE	SWV	0.07	0.07–2.0	3	[67]
AgNWs-PANI/GCE	DPV	0.052	0.6–32	7	[68]
ZnO NPs@fMWCNTs/SPCE	DPV	0.013	0.06–100	7	This work

Abbreviations: Au – gold; GCE – glassy carbon electrode; SDV – semi-derivative voltammetry; Co_3O_4 – cobalt oxide; SWV – square wave voltammetry; HA-NP – hydroxyapatite nanopowder; β-CD/RGO – β cyclodextrin functionalized reduced graphene oxide; GC-UNFE – uniform nanoparticle film electrode of glass carbon; FeO_x/TiO_2@mC – iron oxide and titanium dioxide embedded mesoporous carbon; Cu_2O-Pt RRDE – cuprous oxide modified platinum rotating ring-disk electrode; Au-Cu NPs – gold copper alloy nanoparticles; nAg-chitosan – chitosan stabilized silver nanoparticles; AgNWs-PANI – silver nanowire-polyaniline.

the relative current response of 4-NP at ZnO NPs@fMWCNTs/SPCE in the presence of aforementioned interfering species. From the figure, it is evident that the proposed sensor exhibits good selectivity in the detection of 4-NP as the effect of interfering species on 4-NP peak current response is negligible. In other words, relative error in current response of 4-NP is less than 5.5% indicating a good anti-interference property for ZnO NPs@fMWCNTs based sensor.

Excellent reproducibility is a remarkable trait of an efficient electrochemical sensor. Hence, evaluation of reproducibility of proposed sensor based on ZnO NPs@fMWCNTs is important. We have carried out reproducibility experiment by independently fabricating 10 identical ZnO NPs@fMWCNTs/SPCEs and measuring its peak current in existence of 4-NP. Fig. 10A represents the cathodic peak current responses for 10 identical ZnO NPs@fMWCNTs/SPCEs. We can see that the current responses of all the considered SPCEs are almost the same without much variance and resulted in a small RSD of 3.33%. From this observation, it is apparent that ZnO NPs@fMWCNTs based sensor has good reproducibility property.

We have assessed repeatability of ZnO NPs@fMWCNTs based sensor in this work. For the repeatability evaluation, we have measured 10 successive cathodic peak current responses using the same modified electrode in presence of 4-NP. Fig. 10B depicts peak current responses during the successive measurements. The estimated RSD is just 2.12% revealing the excellent repeatability for the proposed sensor.

3.2.6. Detection of 4-NP in real samples

To examine practical feasibility of developed sensor based on ZnO NPs@fMWCNTs in 4-NP determination, we have carried out real sample analysis experiment in this work. The DPV response of ZnO NPs@fmwcnt/SPCE in different water samples is evaluated as part of this experiment. We have adopted standard addition method for DPV analysis. The real samples used to examine practical feasibility include tap water and river water. We have calculated RSD and recovery values of 4-NP in both water samples, which are given in Table 2. When we analyze the tabulated results from this experiment, we can find that RSD values for the water samples used in this experiment are in 1.94% to 2.79% range. Furthermore, recovery values are in the range of 99.33% to 101.33%. The low RSD values and recovery values with small variance we obtained for the water samples indicate the good practical feasibility of developed sensor based on ZnO NPs@fmwcnt/SPCE towards efficient determination environmental pollutant 4-NP.

4. Conclusions

A highly sensitive electrochemical sensor for detection of hazardous pollutant 4-NP was successfully developed in this work. We have synthesized novel 3D flower-like ZnO NPs using laser-assisted technique and ZnO NPs@fmwcnt nanocomposite was prepared using sonochemical process. Characterizations such as XRD, SEM, HRTEM, Raman spectrum, FT-IR spectrum, and UV–Vis spectrum of ZnO NPs, fMWCNTs, and ZnO NPs@fmwcnt nanocomposite were evaluated as part of this work. ZnO NPs@fmwcnt/SPCE was used for the electrochemical investigations using cyclic voltammetry and effect of pH, scan rate, and concentration were evaluated. DPV technique was employed in the precise detection of 4-NP and we have achieved high sensitivity and very low LOD in a wide linear range for the proposed sensor based on ZnO NPs@fmwcnt/SPCE. Further investigations including selectivity, stability, repeatability, and reproducibility were carried out to analyze the performance of proposed sensor. The experimental results for the aforementioned investigations showcased excellent performance of developed sensor towards the detection of 4-NP. The results from the real sample analysis experiment conducted in different water samples substantiated the practical feasibility of developed sensor. Hence, we

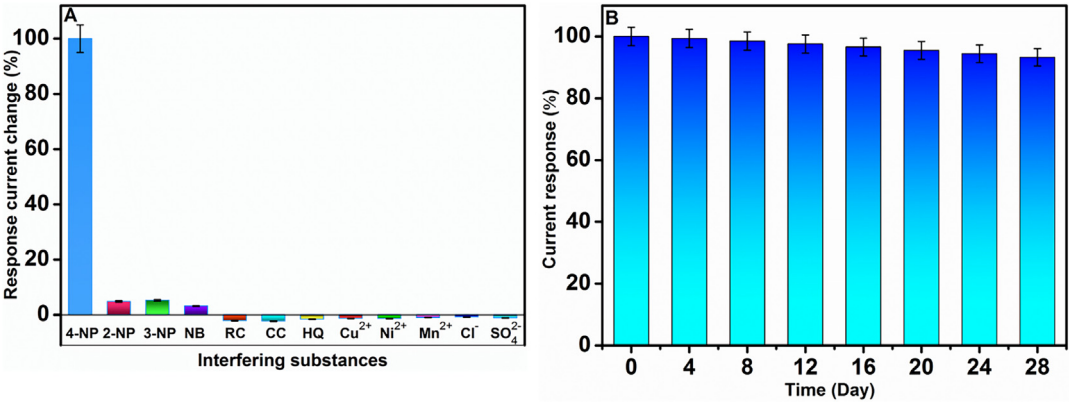

Fig. 9. (A) Interference analysis of ZnO NPs@fMWCNTs based sensor. (B) Monitoring of current response for the stability analysis of ZnO NPs@fMWCNTs based sensor for 28 days. Stability is a salient feature for efficient electrochemical sensors and hence we have conducted experiment to assess stability of proposed sensor based on ZnO NPs@fMWCNTs. To this end, DPV response of sensor was recorded and closely monitored the change in its reduction peak current response over a period of 28 days. The graph representing peak current during 28 days continuous monitoring is given in Fig. 9B. A drop of merely 6.7% in the current response was noted after 28 days storage of the proposed electrochemical sensor indicating a very high stability.

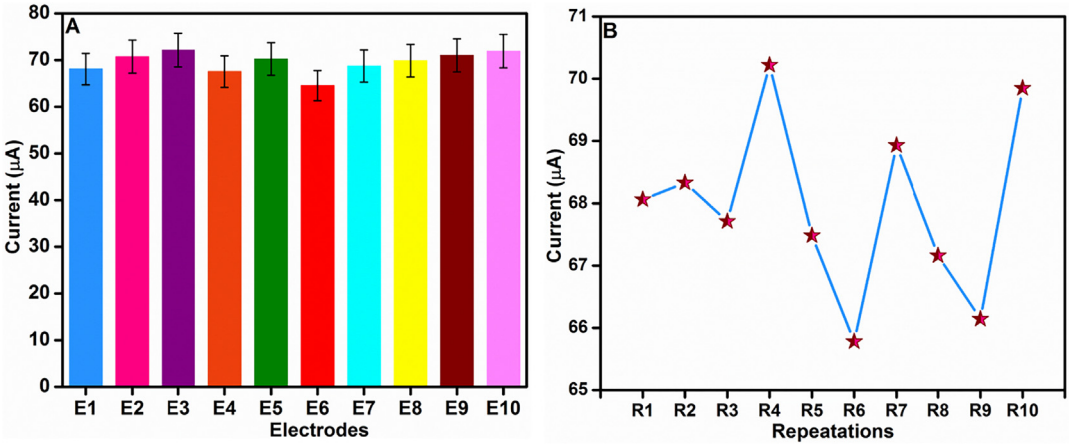

Fig. 10. (A) Reproducibility property investigation of ZnO NPs@fMWCNTs based sensor. (B) Repeatability property investigation of ZnO NPs@fMWCNTs based sensor.

Table 2
Detection of 4-NP in water samples using ZnO NPs@fmwcnt/SPCE.

Sample	Added (μM)	Found (μM)	Recovery (%)	RSD[k] (%)
Tap Water	5	4.96	99.33	2.02
	10	10.13	101.33	2.53
	20	20.05	100.25	1.94
River Water	5	5.01	100.27	2.37
	10	10.04	100.43	2.15
	20	20.21	101.05	2.79

[k]Relative standard deviation of 3 measurements.

conclude that ZnO NPs@fmwcnt nanocomposite is an apt material for sensitive detection of hazardous pollutant 4-NP.

Conflicts of interest

There are no conflicts to declare.

Acknowledgement

This work is supported by the Ministry of Science and Technology, Taiwan, ROC under Grants 105–2221-E–027-114.

References

[1] 4-Nitrophenol, Health and Environmental Effects Profile No. 135, in, U. S. Government Printing Office, U.S. Environmental Protection Agency (EPA), Washington, DC, 1980.
[2] E. Lipczynska-Kochany, Degradation of aqueous nitrophenols and nitrobenzene by means of the Fenton reaction, Chemosphere 22 (1991) 529–536.
[3] Y. Wei, L.-T. Kong, R. Yang, L. Wang, J.-H. Liu, X.-J. Huang, Single-walled carbon nanotube/pyrenecyclodextrin nanohybrids for ultrahighly sensitive and selective detection of p-nitrophenol, Langmuir 27 (2011) 10295–10301.
[4] Z.I. Bhatti, H. Toda, K. Furukawa, p-Nitrophenol degradation by activated sludge attached on nonwovens, Water Res. 36 (2002) 1135–1142.
[5] X. Guo, Z. Wang, S. Zhou, The separation and determination of nitrophenol isomers by high-performance capillary zone electrophoresis, Talanta 64 (2004) 135–139.
[6] M. Miró, A. Cladera, J.M. Estela, V.C. Cerdà, Dual wetting-film multi-syringe flow injection analysis extraction: application to the simultaneous determination of nitrophenols, Anal. Chim. Acta 438 (2001) 103–116.
[7] K.D. Buchholz, J. Pawliszyn, Determination of phenols by solid-phase microextraction and gas chromatographic analysis, Environ. Sci. Technol. 27 (1993) 2844–2848.
[8] R. Belloli, B. Barletta, E. Bolzacchini, S. Meinardi, M. Orlandi, B. Rindone, Determination of toxic nitrophenols in the atmosphere by high-performance liquid chromatography, J. Chromatogr. A 846 (1999) 277–281.
[9] S.J. Pearton, D.P. Norton, K. Ip, Y.W. Heo, T. Steiner, Recent progress in processing and properties of ZnO, Prog. Mater. Sci 50 (2005) 293–340.
[10] D.C. Look, Recent advances in ZnO materials and devices, Mater. Sci. Eng. C 80 (2001) 383–387.
[11] A.B. Djurišić, Y.H. Leung, Optical properties of ZnO nanostructures, small 2 (2006) 944–961.
[12] J. Xiong, Y. Gan, J. Zhu, W. Li, C. Gao, Y. Wei, G. Cheng, Z. Li, S. Dou, Insights into the structure-induced catalysis dependence of simply engineered one-dimensional zinc oxide nanocrystals towards photocatalytic water purification, Inorg. Chem. Front. 4 (2017) 2075–2087.
[13] Ü. Özgür, Y.I. Alivov, C. Liu, A. Teke, M. Reshchikov, S. Doğan, V. Avrutin, S.J. Cho, H. Morkoç, A comprehensive review of ZnO materials and devices, J. Appl. Phys. 98 (2005) 11.
[14] X. Shao, B. Li, B. Zhang, L. Shao, Y. Wu, Au@ ZnO core–shell nanostructures with plasmon-induced visible-light photocatalytic and photoelectrochemical properties, Inorg. Chem. Front. 3 (2016) 934–943.
[15] J. Xiong, W. Li, Y. Gan, Y. Wei, G. Cheng, S. Dou, Z. Li, Extremely rapid engineering of zinc oxide nanoaggregates with structure-dependent catalytic capability towards removal of ciprofloxacin antibiotic, Inorg. Chem. Front. 5 (2018) 2432–2444.
[16] E. Hosono, S. Fujihara, I. Honma, H. Zhou, The fabrication of an upright-standing zinc oxide nanosheet for use in dye-sensitized solar cells, Adv. Mater. 17 (2005) 2091–2094.
[17] K. Kato, P.K. Song, H. Odaka, Y. Shigesato, Study on thermochromic VO2 films grown on ZnO-coated glass substrates for “smart windows”, Jpn. J. Appl. Phys 42 (2003) 6523.
[18] Z.K. Tang, G.K.L. Wong, P. Yu, M. Kawasaki, A. Ohtomo, H. Koinuma, Y. Segawa, Room-temperature ultraviolet laser emission from self-assembled ZnO microcrystallite thin films, Appl. Phys. Lett. 72 (1998) 3270–3272.
[19] Y. Zhang, T.R. Nayak, H. Hong, W. Cai, Biomedical applications of zinc oxide nanomaterials, Curr. Mol. Med. 13 (2013) 1633–1645.
[20] L. Vayssieres, Growth of arrayed nanorods and nanowires of ZnO from aqueous solutions, Adv. Mater. 15 (2003) 464–466.
[21] C.Y. Jiang, X.W. Sun, G.Q. Lo, D.L. Kwong, J.X. Wang, Improved dye-sensitized solar cells with a ZnO-nanoflower photoanode, Appl. Phys. Lett. 90 (2007) 263501.
[22] M. Ahmad, C. Pan, L. Gan, Z. Nawaz, J. Zhu, Highly sensitive amperometric cholesterol biosensor based on Pt-incorporated fullerene-like ZnO nanospheres, J. Phys. Chem. C 114 (2009) 243–250.
[23] Y.J. Xing, Z.H. Xi, Z.Q. Xue, X.D. Zhang, J.H. Song, R.M. Wang, J. Xu, Y. Song, S.L. Zhang, D.P. Yu, Optical properties of the ZnO nanotubes synthesized via vapor phase growth, Appl. Phys. Lett. 83 (2003) 1689–1691.
[24] B. Liu, H.C. Zeng, Hydrothermal synthesis of ZnO nanorods in the diameter regime of 50 nm, J. Am. Chem. Soc. 125 (2003) 4430–4431.
[25] Y. Chen, D.M. Bagnall, H.-J. Koh, K.-T. Park, K. Hiraga, Z. Zhu, T. Yao, Plasma assisted molecular beam epitaxy of ZnO on c-plane sapphire: Growth and characterization, J. Appl. Phys. 84 (1998) 3912–3918.
[26] G.S. Wu, T. Xie, X.Y. Yuan, Y. Li, L. Yang, Y.H. Xiao, L.D. Zhang, Controlled synthesis of ZnO nanowires or nanotubes via sol–gel template process, Solid State Commun. 134 (2005) 485–489.
[27] B.D. Yao, Y.F. Chan, N. Wang, Formation of ZnO nanostructures by a simple way of thermal evaporation, Appl. Phys. Lett. 81 (2002) 757–759.
[28] J. Nause, B. Nemeth, Pressurized melt growth of ZnO boules, Semicond. Sci. Technol. 20 (2005) S45.
[29] M.S. Cao, X.X. Wang, M. Zhang, J.C. Shu, W.Q. Cao, H.J. Yang, X.Y. Fang, J. Yuan, Electromagnetic Response and Energy Conversion for Functions and Devices in Low-Dimensional Materials, Adv. Funct. Mater. 1807398 (2019).
[30] R.H. Baughman, A.A. Zakhidov, W.A. De Heer, Carbon nanotubes–the route toward applications, science 297 (2002) 787–792.
[31] G. Dresselhaus, S. Riichiro, Physical properties of carbon nanotubes, World scientific (1998).
[32] B. Wen, M.-S. Cao, Z.-L. Hou, W.-L. Song, L. Zhang, M.-M. Lu, H.-B. Jin, X.-Y. Fang, W.-Z. Wang, J. Yuan, Temperature dependent microwave attenuation behavior for carbon-nanotube/silica composites, Carbon 65 (2013) 124–139.
[33] W.-L. Song, M.-S. Cao, Z.-L. Hou, X.-Y. Fang, X.-L. Shi, J. Yuan, High dielectric loss and its monotonic dependence of conducting-dominated multiwalled carbon nanotubes/silica nanocomposite on temperature ranging from 373 to 873 K in X-band,

Appl. Phys. Lett. 94 (2009) 233110.
[34] J.H. Zagal, S. Griveau, K.I. Ozoemena, T. Nyokong, F. Bedioui, Carbon nanotubes, phthalocyanines and porphyrins: attractive hybrid materials for electrocatalysis and electroanalysis, J. Nanosci. Nanotechnol 9 (2009) 2201–2214.
[35] R. Zhang, M. Zhang, T. Zhou, T. Zhang, Robust cobalt perforated with multi-walled carbon nanotubes as an effective sensing material for acetone detection, Inorg. Chem. Front. 5 (2018) 2563–2570.
[36] C. Lv, Y. Peng, J. Yang, C. Liu, X. Duan, J. Ma, T. Wang, A free-standing Li 1.2 Mn 0. 54 Ni 0.13 Co 0.13 O 2/MWCNT framework for high-energy lithium-ion batteries, Inorg. Chem. Front., 5 (2018) 3053–3060.
[37] M.-M. Lu, W.-Q. Cao, H.-L. Shi, X.-Y. Fang, J. Yang, Z.-L. Hou, H.-B. Jin, W.-Z. Wang, J. Yuan, M.-S. Cao, Multi-wall carbon nanotubes decorated with ZnO nanocrystals: mild solution-process synthesis and highly efficient microwave absorption properties at elevated temperature, J. Mater. Chem. A 2 (2014) 10540–10547.
[38] Y. Yan, T. Wang, X. Li, H. Pang, H. Xue, Noble metal-based materials in high-performance supercapacitors, Inorg. Chem. Front. 4 (2017) 33–51.
[39] M.-S. Cao, W.-L. Song, Z.-L. Hou, B. Wen, J. Yuan, The effects of temperature and frequency on the dielectric properties, electromagnetic interference shielding and microwave-absorption of short carbon fiber/silica composites, Carbon 48 (2010) 788–796.
[40] R. Torkzadeh-Mahani, M.M. Foroughi, S. Jahani, M. Kazemipour, H. Hassani Nadiki, The effect of ultrasonic irradiation on the morphology of NiO/Co3O4 nanocomposite and its application to the simultaneous electrochemical determination of droxidopa and carbidopa, Ultrason. Sonochem. 56 (2019) 183–192.
[41] L. Esrafili, A. Azhdari Tehrani, A. Morsali, Ultrasonic assisted synthesis of two urea functionalized metal organic frameworks for phenol sensing: a comparative study, Ultrason. Sonochem. 39 (2017) 307–312.
[42] R.D. Senevirathne, L.K. Abeykoon, N.L. De Silva, C.-F. Yan, J. Bandara, Sono-photocatalytic production of hydrogen by interface modified metal oxide insulators, Ultrason. Sonochem. 45 (2018) 279–285.
[43] L.-X. Zuo, L.-P. Jiang, E.S. Abdel-Halim, J.-J. Zhu, Sonochemical preparation of stable porous MnO2 and its application as an efficient electrocatalyst for oxygen reduction reaction, Ultrason. Sonochem. 35 (2017) 219–225.
[44] D. Balram, K.-Y. Lian, N. Sebastian, Ecofriendly synthesized reduced graphene oxide embellished marsh marigold-like zinc oxide nanocomposite based on ultrasonication technique for the sensitive detection of environmental pollutant hydroquinone, Ultrason. Sonochem. 58 (2019) 104650.
[45] J. Zhang, L. Sun, J. Yin, H. Su, C. Liao, C. Yan, Control of ZnO morphology via a simple solution route, Chem. Mater. 14 (2002) 4172–4177.
[46] T.C. Damen, S.P.S. Porto, B. Tell, Raman effect in zinc oxide, Phys. Rev. 142 (1966) 570.
[47] M.S. Dresselhaus, G. Dresselhaus, R. Saito, A. Jorio, Raman spectroscopy of carbon nanotubes, Phys. Rep. 409 (2005) 47–99.
[48] N. Soin, S.S. Roy, S.C. Ray, J.A. McLaughlin, Excitation energy dependence of Raman bands in multiwalled carbon nanotubes, J. Raman Spectrosc. 41 (2010) 1227–1233.
[49] G. Xiong, U. Pal, J.G. Serrano, K.B. Ucer, R.T. Williams, Photoluminesence and FTIR study of ZnO nanoparticles: the impurity and defect perspective, Phys. Status Solidi 3 (2006) 3577–3581.
[50] C. Pholnak, C. Sirisathitkul, S. Suwanboon, D.J. Harding, Effects of precursor concentration and reaction time on sonochemically synthesized ZnO nanoparticles, Mater. Res. 17 (2014) 405–411.
[51] A.B. Lavand, Y.S. Malghe, Synthesis, characterization and visible light photocatalytic activity of nitrogen-doped zinc oxide nanospheres, J. Asian Ceram. Soc. 3 (2015) 305–310.
[52] L. Wang, S. Feng, J. Zhao, J. Zheng, Z. Wang, L. Li, Z. Zhu, A facile method to modify carbon nanotubes with nitro/amino groups, Appl. Surf. Sci 256 (2010) 6060–6064.
[53] A.K. Zak, R. Razali, W.H.A. Majid, M. Darroudi, Synthesis and characterization of a narrow size distribution of zinc oxide nanoparticles, Int. J. Nanomed. 6 (2011) 1399.
[54] F. Hekmat, B. Sohrabi, M.S. Rahmanifar, A. Jalali, Electrophoretic deposition of multi-walled carbon nanotubes on porous anodic aluminum oxide using ionic liquid as a dispersing agent, Appl. Surf. Sci 341 (2015) 109–119.
[55] S. Chatterjee, S.A. Bryan, A.J. Casella, J.M. Peterson, T.G. Levitskaia, Mechanisms of neptunium redox reactions in nitric acid solutions, Inorg. Chem. Front. 4 (2017) 581–594.
[56] D. Balram, K.-Y. Lian, N. Sebastian, A Novel Electrochemical Sensor Based on Flower Shaped Zinc Oxide Nanoparticles for the Efficient Detection of Dopamine, Int. J. Electrochem. Sci. 13 (2018) 1542–1555.
[57] H. Beitollahi, M.M. Ardakani, B. Ganjipour, H. Naeimi, Novel 2, 2′-[1, 2-ethanediylbis (nitriloethylidyne)]-bis-hydroquinone double-wall carbon nanotube paste electrode for simultaneous determination of epinephrine, uric acid and folic acid, Biosens. Bioelectron. 24 (2008) 362–368.
[58] D. Balram, K.-Y. Lian, N. Sebastian, Synthesis of a functionalized multi-walled carbon nanotube decorated ruskin michelle-like ZnO nanocomposite and its application in the development of a highly sensitive hydroquinone sensor, Inorg. Chem. Front. 5 (2018) 1950–1961.
[59] L. Chu, L. Han, X. Zhang, Electrochemical simultaneous determination of nitrophenol isomers at nano-gold modified glassy carbon electrode, J. Appl. Electrochem. 41 (2011) 687–694.
[60] M.M. Shahid, P. Rameshkumar, N.M. Huang, Morphology dependent electrocatalytic properties of hydrothermally synthesized cobalt oxide nanostructures, Ceram. Int. 41 (2015) 13210–13217.
[61] H. Yin, Y. Zhou, S. Ai, X. Liu, L. Zhu, L. Lu, Electrochemical oxidative determination of 4-nitrophenol based on a glassy carbon electrode modified with a hydroxyapatite nanopowder, Microchim. Acta. 169 (2010) 87–92.
[62] Z. Liu, X. Ma, H. Zhang, W. Lu, H. Ma, S. Hou, Simultaneous Determination of Nitrophenol Isomers Based on β-Cyclodextrin Functionalized Reduced Graphene Oxide, Electroanalysis 24 (2012) 1178–1185.
[63] P. Wang, J. Xiao, A. Liao, P. Li, M. Guo, Y. Xia, Z. Li, X. Jiang, W. Huang, Electrochemical determination of 4-nitrophenol using uniform nanoparticle film electrode of glass carbon fabricated facilely by square wave potential pulses, Electrochim. Acta. 176 (2015) 448–455.
[64] M. Wang, Y. Liu, L. Yang, K. Tian, L. He, Z. Zhang, Q. Jia, Y. Song, S. Fang, Bimetallic metal–organic framework derived FeOx/TiO2 embedded in mesoporous carbon nanocomposite for the sensitive electrochemical detection of 4-nitrophenol, Sensor. Actuat. B-Chem. 281 (2019) 1063–1072.
[65] Y.-E. Gu, Y. Zhang, F. Zhang, J. Wei, C. Wang, Y. Du, W. Ye, Investigation of photoelectrocatalytic activity of Cu2O nanoparticles for p-nitrophenol using rotating ring-disk electrode and application for electrocatalytic determination, Electrochim. Acta. 56 (2010) 953–958.
[66] A. Shah, M. Akhtar, S. Aftab, A.H. Shah, H.-B. Kraatz, Gold copper alloy nanoparticles (Au-Cu NPs) modified electrode as an enhanced electrochemical sensing platform for the detection of persistent toxic organic pollutants, Electrochim. Acta. 241 (2017) 281–290.
[67] C.A. de Lima, P.S. da Silva, A. Spinelli, Chitosan-stabilized silver nanoparticles for voltammetric detection of nitrocompounds, Sensor. Actuat. B-Chem. 196 (2014) 39–45.
[68] C. Zhang, S. Govindaraju, K. Giribabu, Y.S. Huh, K. Yun, AgNWs-PANI nanocomposite based electrochemical sensor for detection of 4-nitrophenol, Sensor. Actuat. B-Chem. 252 (2017) 616–623.